Friction **9**(3): 488–501 (2021)
https://doi.org/10.1007/s40544-019-0350-y
ISSN 2223-7690
CN 10-1237/TH
RESEARCH ARTICLE

How the fluorographene replaced graphene as nanoadditive for improving tribological performances of GTL-8 based lubricant oil

Xiaojing CI[1,2], Wenjie ZHAO[1,*], Jun LUO[2], Yangmin WU[1], Tianhao GE[1,2], Qunji XUE[1], Xiulei GAO[3], Zhiwen FANG[3]

[1] *Key Laboratory of Marine Materials and Related Technologies, Zhejiang Key Laboratory of Marine Materials and Protective Technologies, Ningbo Institute of Materials Technology and Engineering, Chinese Academy of Sciences, Ningbo 315201, China*

[2] *School of Materials and Engineering, Shanghai University, Shanghai 200000, China*

[3] *Engineering Technology Research Center of Fluorocarbon Materials, Shandong Zhongshan Photoelectric Materials Co., Ltd., Zibo 255138, China*

Received: 19 August 2019 / Revised: 28 October 2019 / Accepted: 05 December 2019

Abstract: Fluorographene, a new alternative to graphene, it not only inherits the 2-dimensional (2D) layered structure and outstanding mechanical properties, but also possesses controllable C–F bonds. It is meaningful to reveal the evolution processes of the tribological behaviors from graphene to fluorographene. In this work, fluorinated reduced graphene oxide nanosheets (F–rGO) with different degree of fluorination were prepared using direct gas-fluorination and they were added into gas to liquid-8 (GTL-8) base oil as lubricant additive to improve the tribological performance. According to the results, the coefficient of friction (COF) reduced by 21%, notably, the wear rate reduced by 87% with the addition of highly fluorinated reduced graphene oxide (HF–rGO) compared with rGO. It was confirmed that more covalent C–F bonds which improved the chemical stability of HF–rGO resisted the detachment of fluorine so the HF–rGO nanosheets showed less damage, as demonstrated via X-ray photoelectron spectroscopy (XPS), Raman spectra, and transmission electron microscopy (TEM). Meanwhile, the ionic liquid (IL) adsorbed on HF–rGO successfully improved the dispersibility of F–rGO in GTL-8 base oil. The investigation of tribofilm by TEM and focused ion beam (FIB) illustrated that IL displayed a synergy to participate in the tribochemical reaction and increased the thickness of tribofilm during the friction process.

Keywords: reduced graphene oxide; fluorographene; lubricating oil; friction; wear; tribofilm

1 Introduction

Compared with dry friction, lubricant plays a necessary role in machinery, because it not only removes the friction heat but also reduces unnecessary energy loss by reducing the wear and friction [1, 2]. Adding lubricant additive has been considered as an indispensable strategy to enhance the tribological performance of lubricant. As key composition of lubricant, the lubricant additive owns many different functionalities such as anti-wear, anti-oxidation, anti-corrosion, defoaming capability, viscosity modifier, dispersant, and so forth [3, 4]. In the past few years, a lot of 2 dimensional (2D) layered materials including tungsulite (WS_2), molybdenum disulfide (MoS_2), graphitic materials, and hexagonal boron nitride (h-BN) have been added to traditional lubricants to improve their anti-wear and friction reduction performances [5, 6].

Among them, graphene based materials are widely

* Corresponding author: Wenjie ZHAO, E-mail: zhaowj@nimte.ac.cn

used for enhancing the lubrication properties of lubricant as the lubricant additive because they are small sized nanosheets with only a few nanometer thickness and could easily enter the contact surface [7, 8]. For instance, Li et al. [9] fabricated the highly exfoliated reduced graphene oxide nanosheets (rGO) powders using KOH which had a big specific surface area, small particle sizes and a "loose book"-like structure by mixing KOH and GO. The special microstructure made this graphitic materials excellently enhance the tribological performance of poly alpha olefin (PAO-6) and reduce the coefficient of friction (COF) by about 43%. Hu et al. [10] synthesized the covalently grafted graphene which showed a superior dispersion in water using amino-containing poly (ethylene glycol) and graphene, and the sample showed an excellent reduction by 38.5% compared with water. Besides, many researchers focused on modifying graphene and designed some novel graphene based materials [11]. Researches found that many kinds of modified graphene nanosheets displayed an excellent performance of friction reduction and anti-wear as lubricant additives, such as graphene oxide, hydrogenated grapheme, and fluorographene. Yu et al. [12] explored a simple and effective method to synthesize graphene oxide grafted by polyhedral oligomeric silsesquioxane (POSS–GO) and revealed that the lubricant with POSS–GO displayed lower COF and wear rate than pure GTL-8 based oil. Fluoro graphene (FG) as a novel graphene derived material should be emphasized that it has high fluorine density [13]. It not only holds the properties of graphene but also possesses the characteristic of fluoride such as excellent thermal and chemical stability, mechanical strength, and large interlayer distance compared with graphene [14]. It is these properties that endue FG with marvellous tribological performance as lubricant additive [15–17]. For instance, Hou et al. [18] prepared FG by liquid-phase exfoliating from fluorinated graphite, and the friction test results confirmed that FG could greatly enhance the anti-wear property compared with pure base oil. However, to the best of our knowledge, the role of the fluorine content of fluorinated graphene plays in the friction performance is rarely researched. This problem greatly affects the development of fluorinated graphene as an effective lubricant additive and clarifies its applications. Therefore, the tribological performance of fluorinated graphite with different fluorine content deserves further study.

At the present time, the methods for preparing F–G could be mainly divided into two groups: fluorination of G or rGO using F_2, HF, fluoropolymers, or utilizing plasma such as F_2, CF_4, and SF_6, and exfoliation utilizing fluorinated graphite [19, 20]. Compared with F–G synthesized using exfoliation method, F–G prepared by direct gas fluorination has uniform size distribution and similar thickness. Furthermore, F/C ratios of F–G synthesized by gas fluorination could be controlled easily by regulating the heating temperature. It was illustrated that F–G with higher F/C ratio excellently enhanced the friction reduction and anti-wear properties as lubricant additive because there were more covalent C–F bonds in C–F bonds which could ensure a steady chemical properties during the friction process. On the other hand, the size of F–G was reduced with the increase of F/C ratio because of the special properties of synthesizing method. The small size made it possible for F–G to enter the contact area easily, and thus improving the tribological properties of F–G.

In this work, we synthesized F–G with distinct F/C ratios using direct fluorination of rGO using F_2/N_2 mixture, and studied tribological behaviors with the change of fluorination degree of F–G. Furthermore, it was illustrated that the higher fluorination degree could enhance the tribological properties of F–G. As a result, it was found that HF–rGO displayed excellent tribological performance as lubricant additive. We systematically investigated the tribological behaviors of F–G and such observations of F–G provided a friction mechanism for different F/C ratio and supported excellent potential as lubricant additive. Besides, we utilized IL to noncovalently graft the F–G to enhance the dispersibility of F–G in lubricant and probed the role of IL during the friction tests.

2 Experimental section

2.1 Materials

Powder of rGO was provided by Zhongshan Photoelectric Material Co. Ltd., (Shandong, China) and GTL-8 based lubricant oil which mainly composed of hydrocarbon was supplied by the Shell China Ltd. (Shanghai). Quinolizinium ionic liquids [MPIQU][NTf_2]

(IL) was obtained from Guizhou Normal College. All other reagents were purchased from Aladdin Industrial Corporation and used directly.

2.2 Preparation of F–G with different F/C ratios

The F–G was performed in a teflon autoclave using a nitrogen-fluorine mixture (20 vol% F_2). rGO was placed in the teflon autoclave, and the autoclave was filled with a N_2/F_2 mixture heated for 24 h. The heating temperature was set to 50, 100, and 300 °C, and the resulting samples were labeled as sample LF–rGO, MF–rGO, and HF–rGO, respectively, and the F/C ratios were about 0.29, 0.44, and 1.53, respectively.

2.3 Synthesis of IL modified HF–rGO

First, a homogeneous dispersion was acquired by dissolving 50 mg HF–rGO and 100 mg KOH in 100 mL deionized water with ultrasonication for 30 min. Then, 100 mg IL was added to HF–rGO and KOH solution with heating for 24 h at 70 °C and continues stirring, as shown in Fig. 1. Finally, the IL modified HF–rGO was gained by centrifugation, being washed using ethanol and deionized water several times and dried at 60 °C for 8 h in air. For convenience, the resulting sample was labeled as sample HF–rGO+IL.

2.4 Fabrication of F–G with different F/C ratios and HF–rGO+IL oil dispersions

To facilitate the gas to liquid-8 (GTL-8) base oil with LF–rGO, MF–rGO, HF–rGO, and HF–rGO+IL, 3 mg of LF–rGO, MF–rGO, HF–rGO, and HF–rGO+IL were added into 10 mL GTL-8 base oil to ensure the same concentration of 0.3 mg/mL were fabricated. The above mixtures were ultrasonicated for 30 min to prepare homogeneous dispersions.

2.5 Characterization techniques

The physical properties of F–rGO were investigated by X-ray diffraction spectra (XRD D8 ADVANCE, Bruker) and the scans were produced over the 2θ range from 5° to 90° at a scanning rate of 0.09 (°)/s and Raman spectroscopy (Renishaw inVia Reflex) with the laser wavelength of 532 nm. The chemical properties of F–rGO were performed using Fourier transform infrared spectra (FTIR, NICOLET 6700 Fourier transform spectrometer) with the range from 400 to 4,000 cm^{-1} at the revolution of 1 cm^{-1} to determine the chemical structure of F–rGO and HF–rGO+IL. The thermal properties of rGO, LF–rGO, MF–rGO, HF–rGO, and HF–rGO+IL were investigated by thermal gravimetric analysis (TGA) with the heating rate of 10 °C/min from 30 to 800 °C under air atmosphere. An XPS (AXIS ULTRA DLD) was utilized to analyze the chemical element of the F–rGO and HF–rGO+IL. To evaluate the morphology and elemental composition of F–rGO and the cross-section of tribofilm, TEM (Talos F200x) was used. The cross-section of tribofilm was formulated by a focused ion beam scanning electron microscope (FIB-SEM, Auriga). The thickness of F–rGO was gauged by scanning probe microscope (SPM, Dimension 3100) and the size of F–rGO nanosheets were emulated by the zeta potential analyzer (Zetasizer Nano ZS). The morphology of wear traces were

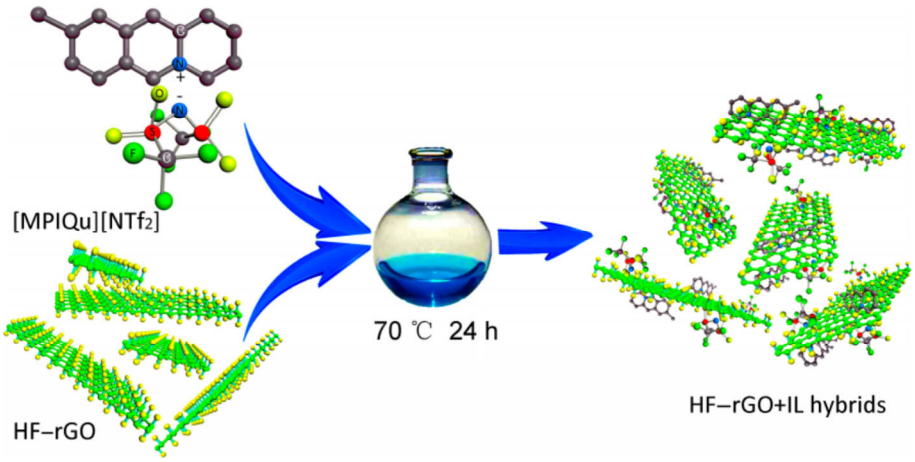

Fig. 1 Schematic illustration of the fabrication of HF–rGO+IL hybrids.

performed with SEM (FEI Quanta FEG 250) under the working voltage of 20 kV and the magnification of 200× and 800×.

UMT-3 (Bruker-CETR, USA) was chosen to evaluate the tribological performances of F–rGO and F–rGO+IL as GTL-8 base oil lubricant nanoadditives. In each test, commercially available silicon nitride (Si_3N_4) balls with a diameter of 3 mm slide reciprocally under a sliding frequency of 2 Hz and a point load of 10 N against a polished 316L for 30 min. The COF was recorded *in situ* by UMT-3 tribometer. For each specimen, at least three times tests were repeated with the same condition to get the repeatability of the data. Before each friction experiment, the friction pairs were all ultrasonically cleaned by ethanol. After the tribological test, all sliding surfaces were washed by ethanol using ultrasonication and the wear scars were measured by Alpha-Step IQ profiler and 3D laser scanning confocal microscopy (VK-X200K) to gauge the wear traces depth and wear scars profiles.

3 Results and discussion

3.1 Structure and morphology of F–rGO

The content of fluorine displayed a great effect on the color of F–rGO. rGO as the raw material showed a black color, while rising the content of fluorination led to a white color for HF–rGO (in this work, the F/C ratio of HF–rGO was 1.53 proved by XPS and was defined to be fully fluorinated graphene according to Nair et al. [41]). Figure S1(a) (in Electronic Supplementary Material (ESM)) showed the optical photos of powdery rGO and F–rGO, and GTL-8 base oil mixed with rGO, LF–rGO, MF–rGO, HF–rGO, and HF–rGO+IL. The color of HF–rGO was white while rGO, LF–rGO, and MF–rGO almost displayed no obvious difference. To test if the addition of IL would enhance the dispersibility of HF–rGO in GTL-8 base oil, a solution of 0.5 mg/mL HF–rGO and HF–rGO+IL in GTL-8 was prepared and then measured using laser light scattering. Figure S1(b) in ESM showed the optical images of the solutions after being kept at room temperature for 7 days compared with freshly prepared mixtures of HF–rGO and HF–rGO+IL. Few aggregation was noticed for HF–rGO+IL according to few reduced intensity of Tyndall effect. However, HF–rGO displayed an obvious aggregation because of the severely reduced scattering intensity. With aim to investigate the dispersibility of HF–rGO and HF–rGO+IL in lubricant, we shook lubricant oil contained HF–rGO and HF–rGO+IL and then measured the mixtures using laser light scattering. It was interesting to observe that the intensity of Tyndall effect of mixture contained HF–rGO+IL was obviously higher than HF–rGO, which illustrated that HF–rGO+IL displayed a better dispersibility in lubricant compared with HF–rGO.

The layered structures of F–rGO were investigated by XRD pattern as shown in Fig. 2(a). Based on Bragg's law, the reduced value of 2θ indicated the larger interplanar distance for F–rGO. According to Fig. 2(a), the (001) diffraction peak of rGO, LF–rGO, MF–rGO, and HF–rGO were located at 2θ =16.84°, 13.95°, 13.86°, and 13.52°, respectively. Then, the interplanar distance of rGO, LF–rGO, MF–rGO, and HF–rGO were calculated to be 0.41, 0.61, 0.62, and 0.65 nm, respectively. These data clearly illustrated that the increased degree of fluorination would give rise to large interplanar distance due to electrostatic repulsive force originated from fluorine atom [21], which meant an easier shear capability to enhance lubricant performance of HF–rGO [22].

Thermal stabilities of F–rGO with various fluorine content were displayed using DTG curve shown in Fig. 2(b). All curves in Fig. 2(b) could be divided into four weight loss steps for different thermal stability process. At the first stage from 0 to 200 °C, all samples displayed thermal stability. There were a broad weight loss which was observed for LF–rGO and MF–rGO, it may be attributed to the thermal detachment of residual oxygen-containing functional group and a few C–F bonds with low stability such as ionic C–F bonds. Meanwhile, rGO and HF–rGO still showed thermal stability at the second step from 200 to 550 °C. At the third stage from 550 to 700 °C, all samples were found with a sharp weight loss due to the detachment of fluorine from F–rGO [23], while it was found that the corresponding temperature of maximum decomposition rate was increased with degree of fluorination. This illustrated clearly that thermal stability of F–rGO was in closely positive correlation with the fluorine content [24].

FTIR spectra were utilized for investigating the chemical structures of F–rGO as shown in Fig. 2(c).

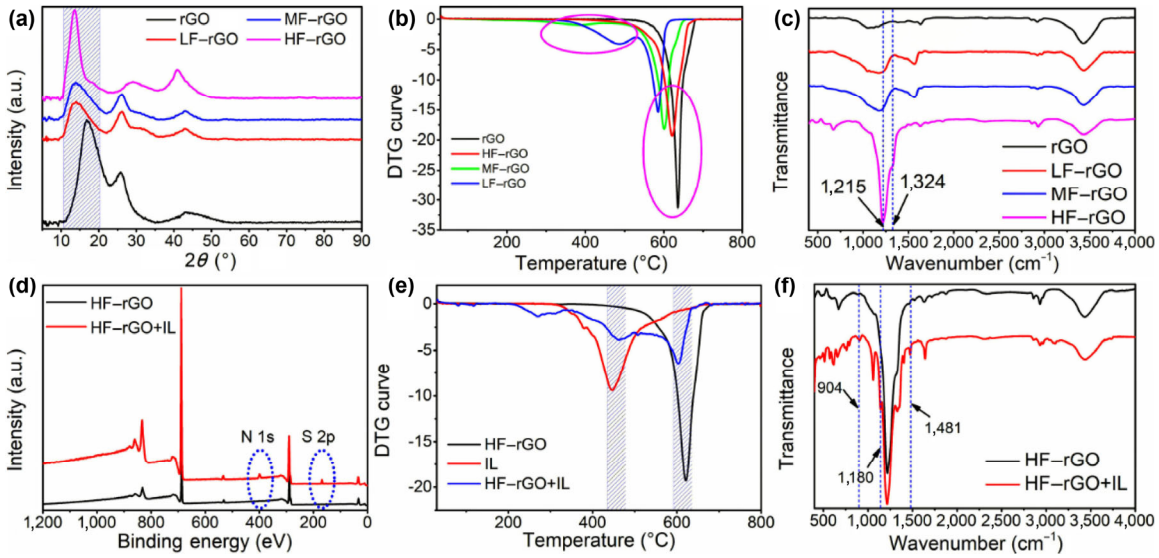

Fig. 2 (a) XRD patterns of rGO, LF–rGO, MF–rGO, and HF–rGO. (b) DTG curves of LF–rGO, MF–rGO, and HF–rGO. (c) FTIR spectra of rGO, LF–rGO, MF–rGO, and HF–rGO. (d) XPS spectra of HF–rGO and HF–rGO+IL. (e) DTG curves of HF–rGO and HF–rGO+IL. (f) FTIR spectra of HF–rGO and HF–rGO+IL.

It was obvious that HF–rGO showed a sharp peak at 1,215 cm^{-1}, which was attributed to the stretching vibration of C–F bonds [25] while rGO showed almost none peak at 1,215 cm^{-1}. The peak at 1,324 cm^{-1} was assigned to the stretching vibration of C–F located at the margin of nanosheet and was only displayed by HF–rGO [26].

To further investigate the HF–rGO and HF–rGO+IL hybrid nanomaterial, XPS, TGA, and FTIR were utilized as shown in Figs. 2(d)–2(f), respectively. Figure 2(d) illustrated that nitrogen peak and sulfur peak were clearly observed for HF–rGO+IL at 401.6 and 168.2 eV, respectively, which may be originated from the adsorbed NTf_2^-. Furthermore, it was clearly that DTG curve of HF–rGO+IL displayed two weight loss stages which was due to the different thermal decomposition steps (Fig. 2(e)). From about 300 to 500 °C, IL displayed a sharp weight loss, meanwhile, HF–rGO+IL also showed a weight loss which illustrated that the IL molecules adsorbing the HF–rGO. Another weight loss step from 500 to 700 °C for HF–rGO+IL was attributed to fluorine detachment. FTIR spectra of the HF–rGO and HF–rGO+IL were shown in Fig. 2(f). The peaks of HF–rGO+IL appeared at 904, 1,180, and 1,481 cm^{-1} were ascribed to S–N, $–SO_2$ [27], and C=N in the quinoline ring. These results clearly demonstrated that IL was successfully grafted on HF–rGO.

With the aim to further measure element composition and chemical bond of various fluorine content, XPS spectra were utilized. C 1s, F 1s, and O 1s peaks were clearly observed from the XPS survey spectra which located at about 284.5, 687, and 533 eV, respectively, as shown in Figs. $3(a_1)$–$3(d_1)$. Chemical composition of F–rGO with different degree of fluorination calculated by XPS spectra was listed in Table 1. Furthermore, the high resolution XPS spectra of C 1s were displayed in Figs. $3(a_2)$–$3(d_2)$. The C 1s spectrum was deconvoluted to some symmetrical carbon bonds, such as C–C, C=C, C–O, covalent C–F, semi-ionic C–F, and ionic C–F. The peaks at 285.3 and 284.5 eV were attributed to C–C bond and C=C bond, respectively [28–31]. Besides, the peaks located at 291, 289, and 287 eV were ascribed to the covalent C–F, semi-ionic C–F, and ionic C–F, respectively. It could be clearly observed that the content of covalent C–F was increased with the higher degree of fluorination, which would enhance the chemical stability and keep an easier shear capability for HF–rGO to enhance the lubricant properties. Different types of C–F bonds were shown in Fig. 3(e).

According to TEM images, AFM images, and size measured by dynamic light scatteringin of rGO, LF–rGO, MF–rGO, and HF–rGO shown in Fig. S2 (in ESM). There were no obvious distincts obtained from TEM images. rGO, LF–rGO, MF–rGO, and HF–rGO

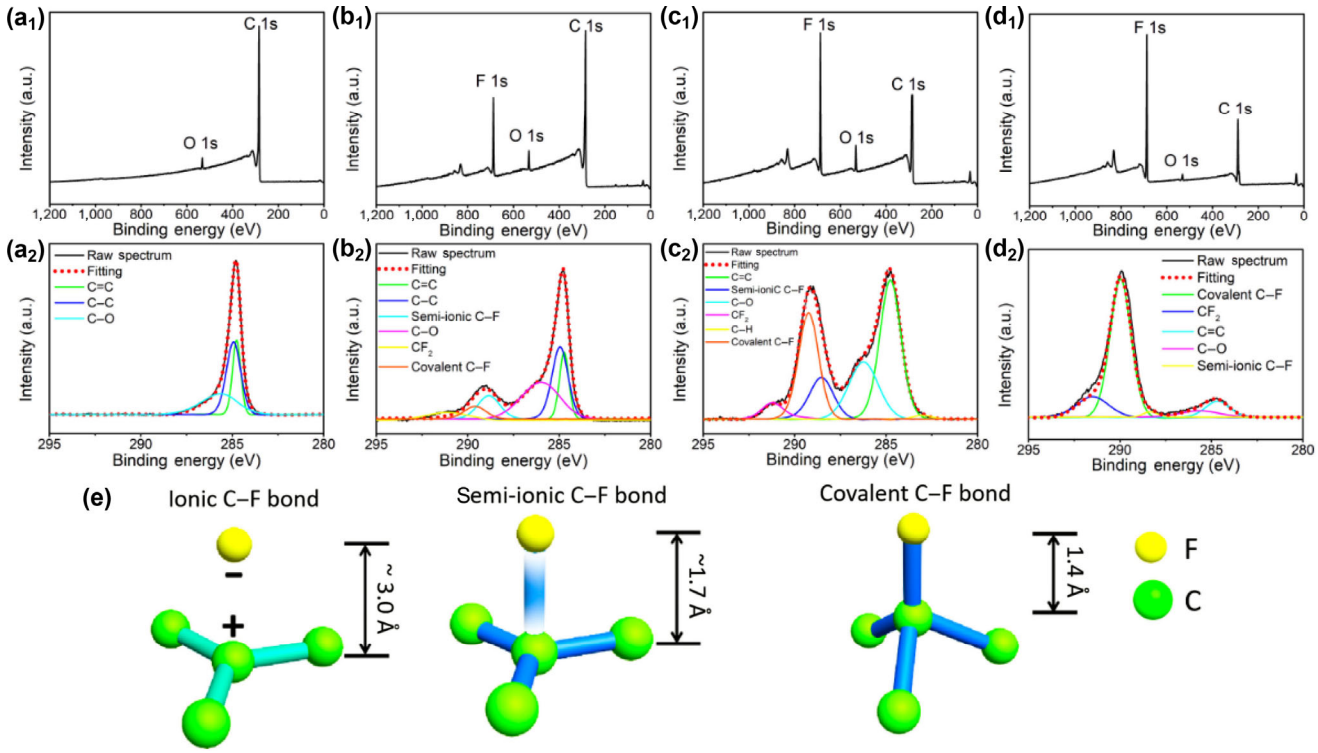

Fig. 3 Full spectrum of (a_1) rGO, (b_1) LF–rGO, (c_1) MF–rGO, and (d_1) HF–rGO. High-resolution XPS spectra of (a_2) rGO, (b_2) LF–rGO, (c_2) MF–rGO, and (d_2) HF–rGO. (e) Length of C–F bonds.

Table 1 Chemical composition of rGO and F–rGO with different degree of fluorination.

Sample	Atomic concentration (%)			
	C	F	O	F/C
rGO	95.12	—	4.88	0
LF–rGO	69.83	20.74	9.43	0.29
MF–rGO	64.83	28.55	6.62	0.44
HF–rGO	38.44	59.07	2.49	1.53

showed an average thickness of 2.08, 2.48, 3.34, and 2.25 nm, respectively. Based on above-mentioned interplanar distance according to XRD pattern of (001) calculated by Bragg's law, the thickness of rGO, LF–rGO, MF–rGO, and HF–rGO were six to seven layers, four to five layers, five to six layers, and three to four layers, respectively. It illustrated that the rGO layers were reduced with the increase of fluorine content. The values of rGO, LF–rGO, MF–rGO, and HF–rGO were 1,041, 967, 692.5, and 644 nm, respectively. Thus, we could draw a conclusion that the size of F–rGO decreased with the increasing degree of fluorination which was related to more harsh surroundings needed for the higher degree of fluorination [32]. The property made HF–rGO enter the friction surface easily to enhance the tribological properties.

3.2 Lubrication performance of GTL-8 base oil mixed with rGO, LF–rGO, MF–rGO, HF–rGO, and HF–rGO+IL

With the aim to study the tribological properties of five samples as lubricant additives, a series of GTL-8 lubricants mixed with rGO, LF–rGO, MF–rGO, HF–rGO, and HF–rGO+IL were prepared. The COF, the cross-sectional profiles of the wear tracks, and wear rate of Si_3N_4 against 316L at 10 N with a frequency of 2 Hz were provided in Fig. 4. It could be observed that the COF ended at 0.165 for pure oil, 0.141 for rGO, 0.133 for LF–rGO, 0.118 for MF–rGO, and 0.114 for HF–rGO (Fig. 4(a)). It was obvious that all the COF of GTL-8 base oil mixed with rGO and F–rGO displayed significant reduction compared with pure oil. Meanwhile, the lubricant mixed with HF–rGO showed obvious reduction in COF compared with GTL-8 mixed with rGO, which illustrated that the property of

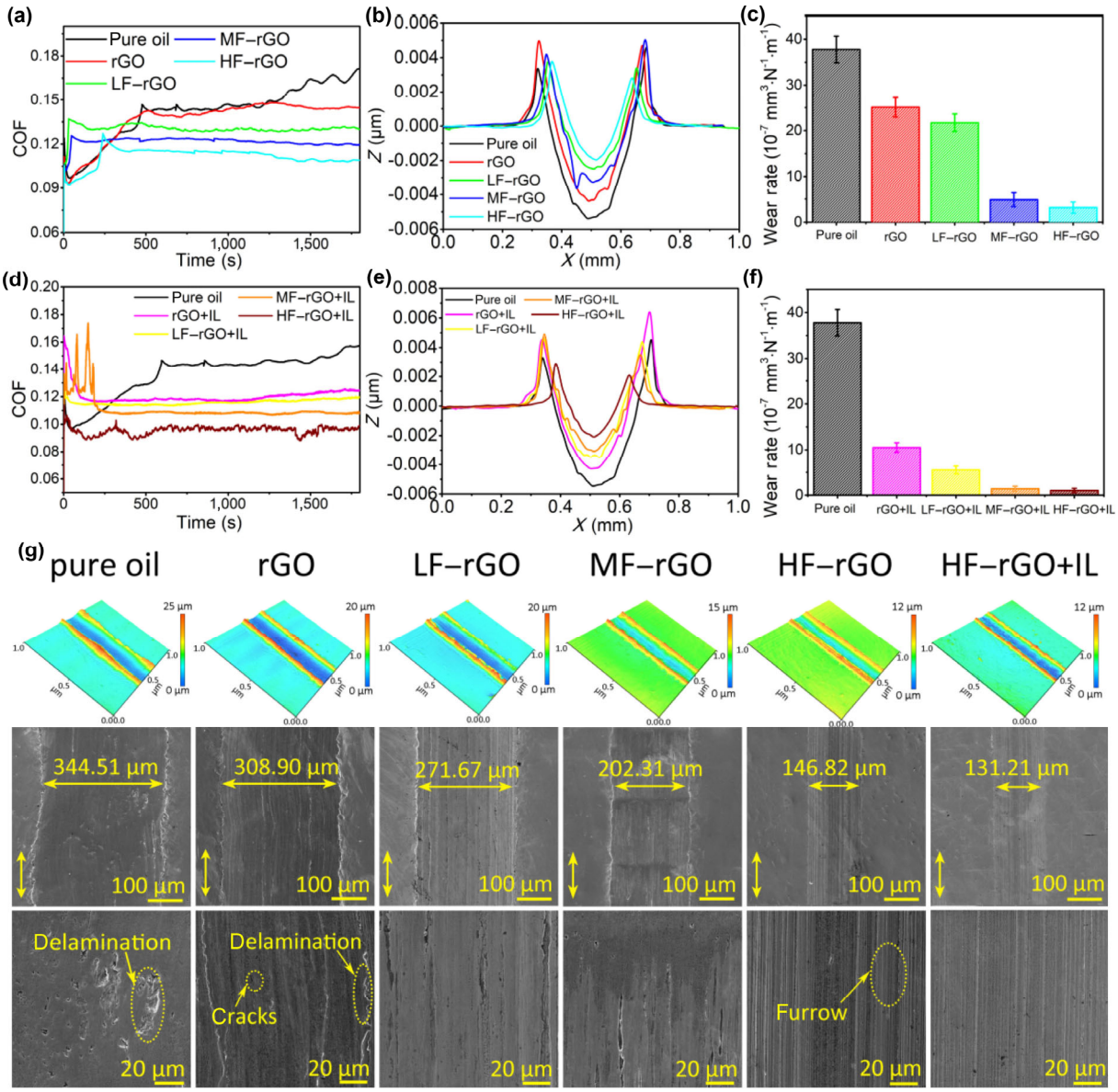

Fig. 4 Tribological properties of GTL-8 based oil contained rGO, LF–rGO, MF–rGO, and HF–rGO: (a) Mean COF under 10 N, 2 Hz, and 30 min, (b) cross-sectional profiles of the wear tracks, and (c) wear rate. Tribological properties of GTL-8 based oil contained rGO+IL, LF–rGO+IL, MF–rGO+IL, and HF–rGO+IL. (d) mean COF under 10 N, 2 Hz, and 30 min, (e) cross-sectional profiles of the wear tracks, (f) wear rate, (g) 3D profiles and SEM images with magnification of 200× and 800× of the wear scars on 316 steel lubricated with pure oil, rGO, LF–rGO, MF–rGO, HF–rGO, and HF–rGO+IL.

friction reduction showed an improvement with the increasing degree of fluorination. According to the cross-sectional profiles of the wear tracks (Fig. 4(b)), both the depth and the width of wear surface for HF–rGO were the smallest among all the samples. For pure oil, the depth and width of wear track were 0.56 and 0.34 mm, respectively. With the addition of rGO, the depth and width of wear track on 316L were decreased to 0.42 and 0.31 mm, respectively. The depth and width of wear track for lubricant with HF–rGO were reduced to 0.21 and 0.14 mm, respectively. The wear rate *Ws* was obtained by the Eq. (1) [33].

$$Ws = \frac{V}{F \cdot L} \tag{1}$$

where V is the friction volume during the tribology test, F is the point load, and L is the whole distance. Calculations displayed that the wear rate of rGO,

LF–rGO, MF–rGO, HF–rGO, and HF–rGO+IL were 25.1×10^{-7}, 21.7×10^{-7}, 4.86×10^{-7}, 3.15×10^{-7}, and 3.02×10^{-7} $mm^3/(N \cdot m)$ as shown in Fig. 4(c). There seemed to be a trend that the anti-wear performance got an enhancement with the higher fluorine content. In conclusion, the COF of GTL-8 contained HF–rGO presented a 31% decrease compared to pure oil and the wear rate presented a 90% decrease. Furthermore, the COF of HF–rGO was reduced by 21% and the wear rate was reduced by 87% compared with rGO. These results could be attributed to smaller size, easier shear capability, and higher chemical stability of HF–rGO as mentioned above.

The tribological performances of HF–rGO+IL were shown in Figs. 4(d)–4(f). It could be observed that both the COF and the wear rate of GTL-8 contained HF–rG+IL were slightly reduced compared with GTL-8 mixed with HF–rGO, which was due to the improved dispersibility of HF–rGO+IL in oil.

To further explore the observed effect of GTL-8 base oil contained rGO and F–rGO for enhancing tribological properties, SEM was used to observe the morphology of wear scars. SEM micrographs of wear traces with magnification of 200× and 800× formed from pure oil, GTL-8 contained rGO, LF–rGO, MF–rGO, HF–rGO, and HF–rGO+IL were shown in Fig. 4(g). It was obvious that the width of wear scars were gradually reduced for that from rGO to HF–rGO as lubricant additive, which further illustrated that higher fluorine content could enhance the anti-wear property of GTL-8. As shown in SEM micrographs with magnification of 800×, it is clear to observe the wavy morphology such as delamination and cracks due to chemical plastic deformation on the worn surface marked by yellow loops. This illustrated that the wear of 316L was reduced with the higher fluorination degree of lubricant additives, meanwhile, the surface of wear traces became smooth. The three dimensional (3D) profiles of wear scars on the 316L vividly displayed that a wider and deeper wear scar formed on the surface lubricated with GTL-8 containing rGO while a narrower and shallower wear scar formed on the surface lubricated with GTL-8 containing HF–rGO. To summarize, the microscopy of worn surface illustrated that the performance of anti-wear was improved as the degree of fluorination increased. The morphology of worn surface for HF–rGO and HF–rGO+IL further illustrated that the HF–rGO+IL could enhance the anti-wear property of GTL-8 base oil compared with HF–rGO due to the noncovalently graft of IL.

3.3 Friction reduction and wear resistance mechanism analysis

The optical micrographs of the wear tracks formed on the surface lubricated with GTL-8 oil containing rGO and HF–rGO were shown in Figs. 5(a_1) and 5(b_1), respectively. It was obvious that the width of wear track formed on the surface lubricated with HF–rGO was much narrower than that with rGO, besides, it also displayed more slight wear area (area with light color) compared with that lubricated with rGO. To further reveal the phenomenon, the wear area whose size was 20 μm × 20 μm was observed using Raman spectral maps with the characteristic Raman shift at 1,600 cm^{-1}. The Raman mapping image shown in Fig. 5(a_2) clearly displayed the strong intensity at 1,600 cm^{-1} which was attributed to the G band of rGO. It was clearly displayed that no obvious G band was found compared with that lubricated with HF–rGO. The Raman mapping image of wear track lubricated with HF–rGO with the same condition was shown in Fig. 5(b_2). It was illustrated that HF–rGO showed less structure defects [34] during friction process due to the chemical stability of HF–rGO. On the other hand, it could be owing to the small size of HF–rGO which helps HF–rGO enter the contact surface more easily during the friction process. In order to validate above explanation, Raman spectrum images of rGO and HF–rGO before and after friction tests were displayed in Figs. 5(a_3) and 5(b_3). The rGO showed acquired defects during friction process, as proved by the increase of I_D/I_G from 0.43 to 1.14 after sliding process [35]. However, the increase of I_D/I_G for HF–rGO was less compared with rGO, which further illustrated that HF–rGO displayed a higher chemical stability because of more covalent C–F bond contained in the HF–rGO.

The surface microstructure and element of LF–rGO, MF–rGO, and HF–rGO before and after tribological tests were investigated by TEM as shown in Fig. 6. Before test, the LF–rGO, MF–rGO, and HF–rGO sheets

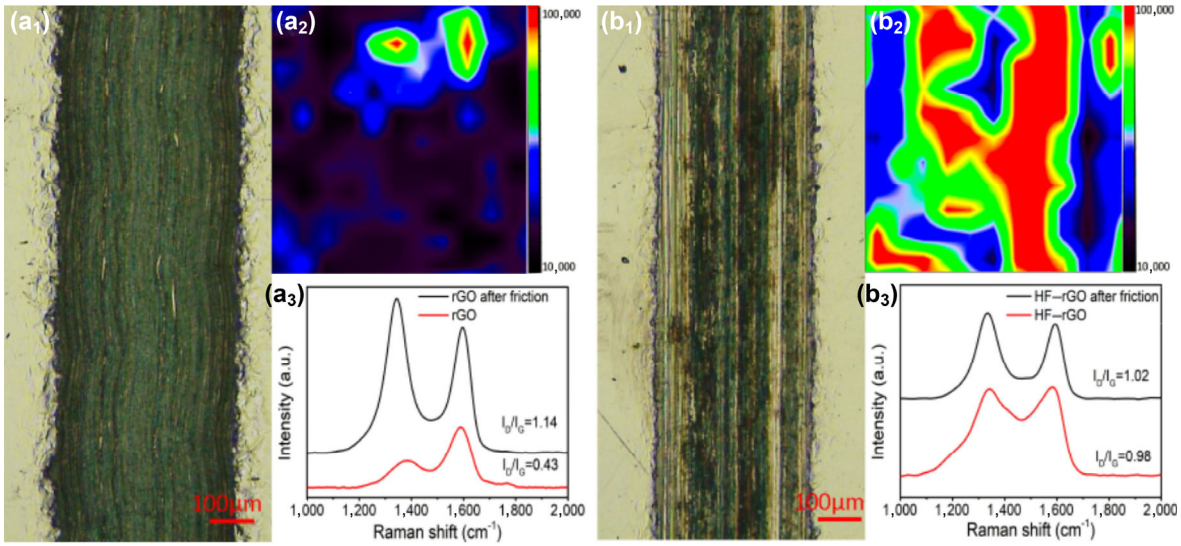

Fig. 5 Optical micrographs of worn surface on 316L lubricated by GTL-8 contained (a_1) rGO and (b_1) HF–rGO. Raman mapping image of worn surface on 316L lubricated by GTL-8 contained (a_2) rGO and (b_2) HF–rGO. Raman spectra of worn surface on 316L lubricated by GTL-8 contained (a_2) rGO and (b_2) HF–rGO.

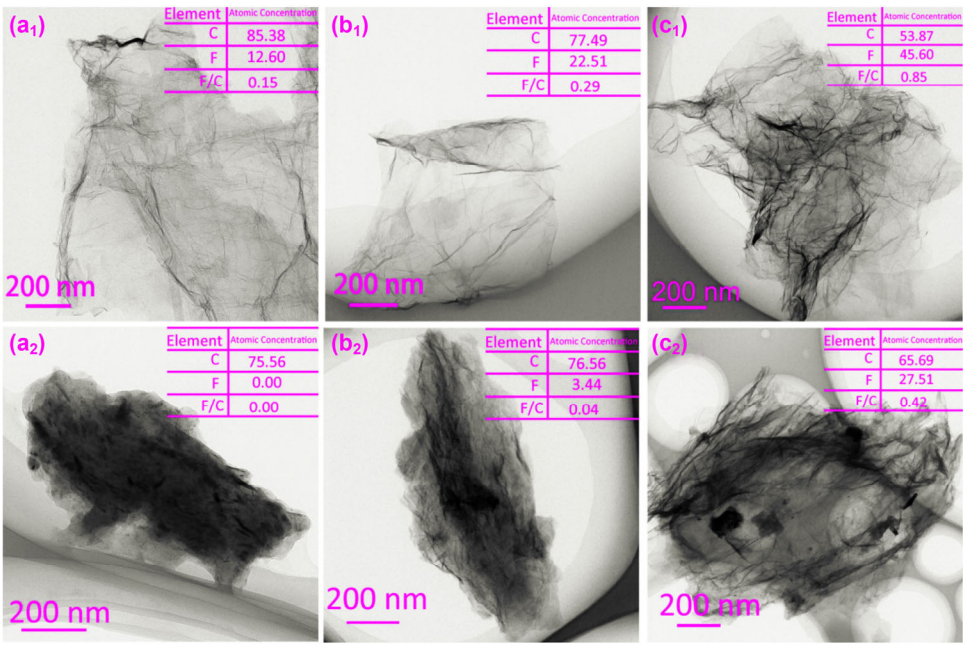

Fig. 6 TEM images of (a_1) LF–rGO, (b_1) MF–rGO, and (c_1) HF–rGO before friction test, (a_2) LF–rGO, (b_2) MF–rGO, and (c_2) HF–rGO after friction test. The inset tables were EDS data of wear debris.

(Figs. 6(a_1), 6(b_1) and 6(c_1)) displayed like a transparent crumpled cloth with F/C increased from 0.15 to 0.85. The surface microstructure of wear debris from the wear tracks lubricated with GTL-8 containing LF–rGO, MF–rGO, and HF–rGO were observed in Figs. 6(a_2), 6(b_2) and 6(c_2)). It was obvious that LF–rGO and MF–rGO displayed severe aggregation with small size and became a chunk with almost none wrinkle while HF–rGO could be found with less aggregation with many dark areas and winkle [36]. These results illustrated that LF–rGO and MF–rGO were severely damaged during the friction process compared with HF–rGO. To further research the mechanism of these phenomenon, the element concentration of wear debris after friction tests was evaluated. Compared with the F/C before friction, all the F/C after tests decreased

because of the detachment of fluorine during sliding process; however, the minimal reduction of F/C was displayed by HF–rGO due to the high chemical stability resulted from strong covalent C–F bond.

In conclusion, HF–rGO displayed excellent tribological properties as lubricant additive compared with rGO, LF–rGO, and MF–rGO. There were three main factors: First, the small size caused by the severe fluorination process made the HF–rGO sheets enter the contact area of friction easily; second, HF–rGO displayed a large interlayer spacing because high degree of fluorination made more fluorine enter interlayer of rGO, which improved the shear capability of HF–Rgo; besides, compared with other samples, HF–rGO showed a higher chemical stability originated from the strong covalent C–F bond, which confirmed that the fluorine atomic detached difficultly during the friction process. It meant that HF–rGO still showed high degree of fluorination after tribological tests, which could bring great crack resistance capability caused by the reduced out-plane stress and in-plane stiffness [11]. The corresponding schematic sketch was shown in Fig. 7.

To research the role of the IL played during the friction test, a further research of the morphology and composition for tribofilm were utilized by the FIB and TEM to analyze the cross-section of wear track. Obviously, protective tribofilm with a thickness of 50 nm evenly formed on the 316L substrate after friction tests with lubricant of GTL-8 containing HF–rGO as shown in Fig. 8(a_1). The energy dispersive spectrometer (EDS) linear analysis along the straight lines in yellow was shown in Fig. 8(a_2). The element of F was affluent in the area of tribofilm, which illustrated that the tribofilm formed by HG–rGO was consisted of FeF_2 with anti-scrach property [37]. To deeply understand the tribological properties of HF–rGO+IL as lubricant additives, a close TEM image was observed in Figs. 8(b_1) and 8(b_2). Clearly, protection tribofilm with a thickness of 50 nm formed on the wear surface which was supposed to be that the presence of IL could improve the thickness of protective tribofilm. The EDS linear analysis along the straight lines in yellow suggested that the tribofilm was consisted with Fe, O, F, N, and S likely mixture of FeO_x, FeF_2, FeN, and FeS [38–40]. These illustrated that IL participated in the formation of tribofilm.

4 Conclusions

In this study, F–rGO nanosheets with different degree of fluorination were prepared using direct gas-flurination utilizing F_2/N_2 mixture, and they were added into GTL-8 base oil as lubricant additive to improve the tribological performance. Compared with pure lubricant oil, the COF was reduced by 30% and wear rate was reduced by 90% with the addition of HF–rGO. Meanwhile, compared with GTL-8 containing rGO, the COF was reduced by 21% and wear rate was reduced by 87% with the addition of HF–rGO. The results were attributed to the excellent tribological properties of HF–rGO. In regard to the tribological mechanism, three main factors were drawn: 1) the nanosheets with small size entered contact surface easily, 2) the large interlayer spicing made the sample show great shear capability, and 3) more concentration of covalent C–F bonds which improved

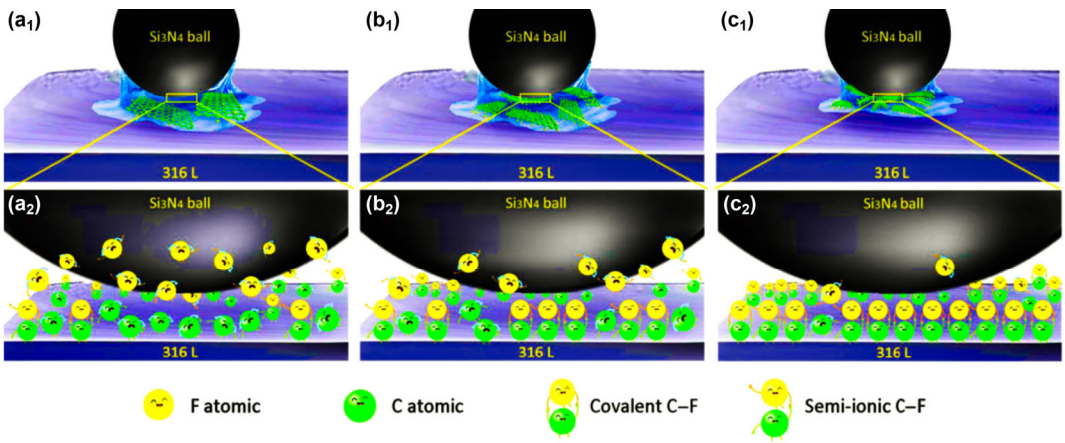

Fig. 7 Schematic sketch of friction mechanism.

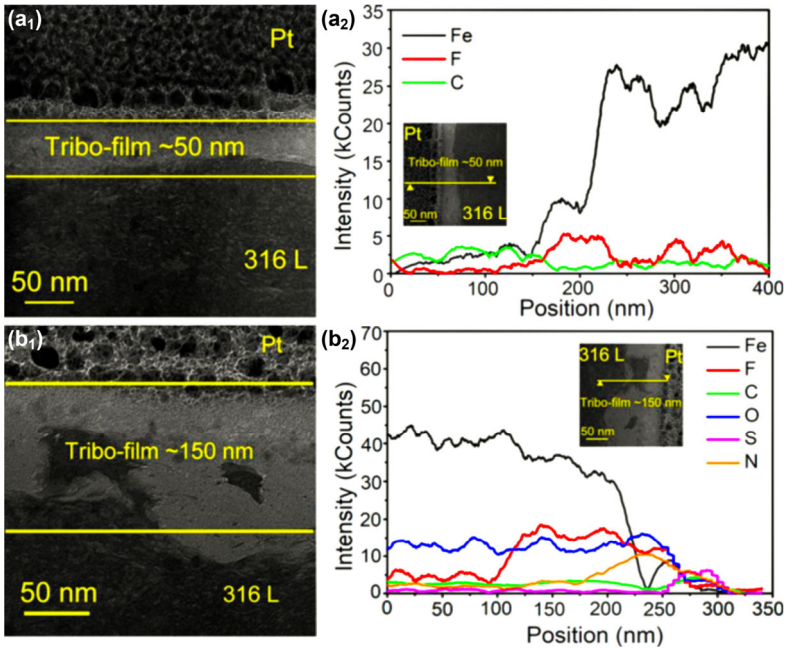

Fig. 8 TEM images of tribofilm formed on wear scar lubricated by GTL-8 contained (a_1) HF–rGO and (b_1) HF–rGO+IL. EDS linear scanning data of tribofilm formed on wear scar lubricated by GTL-8 contained (a_2) HF–rGO and (b_2) HF–rGO+IL.

the chemical stability of HF–rGO resisted the detachment of fluorine so that the HF–rGO sheet displayed the least damage. On the other hand, the IL adsorbed on HF–rGO successfully improved the dispersibility of HF–rGO in the GTL-8 base oil. Furthermore, according to the investigation of tribofilm, IL participated in the tribochemical reaction and increased the thickness of tribofilm during the friction process. This work promised a new vista on fluorinated graphene as lubricant additive in practical application.

Acknowledgements

We express our great thanks to the National Natural Science Foundation of China (51775540), Key Research Program of Frontier Sciences of the Chinese Academy of Sciences (QYZDY-SSW-JSC009), and the Youth Innovation Promotion Association, CAS (2017338).

Electronic Supplementary Material: Supplementary material is available in the online version of this article at https://doi.org/10.1007/s40544-019-0350-y.

References

[1] Holmberg K, Andersson P, Erdemir A. Global energy consumption due to friction in passenger cars. *Tribol Int* **47**: 221–234 (2012)

[2] Ewen J P, Heyes D M, Dini D. Advances in nonequilibrium molecular dynamics simulations of lubricants and additives. *Friction* **6**(4): 349–386 (2018)

[3] Barnes A M, Bartle K D, Thibon V R A. A review of zinc dialkyldithiophosphates (ZDDPS): Characterisation and role in the lubricating oil. *Tribol Int* **34**(6): 389–395 (2001)

[4] Keresztes R, Odrobina M, Nagarajan R, Subramanian K,

Kalacska G, Sukumaran J. Tribological characteristics of cast polyamide 6 (PA6G) matrix and their composite (PA6G SL) under normal and overload conditions using dynamic pin-on-plate system. *Compos B Eng* **160**: 119–130 (2019)

[5] Gao X L, Liu D H, Song Z, Dai K. Isosteric design of friction-reduction and anti-wear lubricant additives with less sulfur content. *Friction* **6**(2): 164–182 (2018)

[6] Le Cao Ky D, Khac B C T, Le C T, Kim Y S, Chung K H. Friction characteristics of mechanically exfoliated and CVD-grown single-layer MoS2. *Friction* **6**(4): 395–406 (2018)

[7] Liu L C, Zhou M, Jin L, Li L C, Mo Y T, Su G S, Li X, Zhu H W, Tian Y. Recent advances in friction and lubrication of graphene and other 2D materials: Mechanisms and applications. *Friction* **7**(3): 199–216 (2019)

[8] Ou J F, Wang J Q, Liu S, Mu B, Ren J F, Wang H G, Yang S R. Tribology study of reduced graphene oxide sheets on silicon substrate synthesized via covalent assembly. *Langmuir* **26**(20): 15830–15836 (2010)

[9] Li Y R, Zhao J, Tang C, He Y Y, Wang Y F, Chen J, Mao J Y, Zhou Q Q, Wang B Y, Wei F, et al. Highly exfoliated reduced graphite oxide powders as efficient lubricant oil additives. *Adv Mater Interfaces* **3**(22): 1600700 (2016)

[10] Hu Y W, Wang Y X, Zeng Z X, Zhao H C, Ge X W, Wang K, Wang L P, Xue Q J. PEGlated graphene as nanoadditive for enhancing the tribological properties of water-based lubricants. *Carbon* **137**: 41–48 (2018)

[11] Fan K, Chen X Y, Wang X, Liu X K, Liu Y, Lai W C, Liu X Y. Toward excellent tribological performance as oil-based lubricant additive: Particular tribological behavior of fluorinated graphene. *ACS Appl Mater Interfaces* **10**(34): 28828–28838 (2018)

[12] Yu B, Wang K, Hu Y W, Nan F, Pu J B, Zhao H C, Ju P F. Tribological properties of synthetic base oil containing polyhedral oligomeric silsesquioxane grafted graphene oxide. *RSC Adv* **8**(42): 23606–23614 (2018)

[13] Yang Z Q, Wang L D, Sun W, Li S J, Zhu T Z, Liu W, Liu G C. Superhydrophobic epoxy coating modified by fluorographene used for anti-corrosion and self-cleaning. *Appl Surf Sci* **401**: 146–155 (2017)

[14] Ko J H, Kwon S, Byun I S, Choi J S, Park B H, Kim Y H, Park J Y. Nanotribological properties of fluorinated, hydrogenated, and oxidized graphenes. *Tribol Lett* **50**(2): 137–144 (2013)

[15] Wang X, Dai Y Y, Gao J, Huang J Y, Li B Y, Fan C, Yang J, Liu X Y. High-yield production of highly fluorinated graphene by direct heating fluorination of graphene-oxide. *ACS Appl Mater Interfaces* **5**(17): 8294–8299 (2013)

[16] Lai W C, Xu D Z, Wang X, Wang Z M, Liu Y, Zhang X J, Li Y L, Liu X Y. Defluorination and covalent grafting of fluorinated graphene with TEMPO in a radical mechanism. *Phys Chem Chem Phys* **19**(35): 24076–24081 (2017)

[17] Robinson J T, Burgess J S, Junkermeier C E, Badescu S C, Reinecke T L, Perkins F K, Zalalutdniov M K, Baldwin J W, Culbertson J C, Sheehan P E, et al. Properties of fluorinated graphene films. *Nano Lett* **10**(8): 3001–3005 (2010)

[18] Hou K M, Gong P W, Wang J Q, Yang Z G, Wang Z F, Yang S R. Structural and tribological characterization of fluorinated graphene with various fluorine contents prepared by liquid-phase exfoliation. *RSC Adv* **4**(100): 56543–56551 (2014)

[19] Feng W, Long P, Feng Y Y, Li Y. Two-dimensional fluorinated graphene: Synthesis, structures, properties and applications. *Adv Sci* **3**(7): 1500413 (2016)

[20] Chronopoulos D D, Bakandritsos A, Pykal M, Zbořil R, Otyepka M. Chemistry, properties, and applications of fluorographene. *Appl Mater Today* **9**: 60–70 (2017)

[21] Zhang X X, Yu L, Wu X Q, Hu W H. Experimental sensing and density functional theory study of H_2S and SOF_2 adsorption on Au-modified graphene. *Adv Sci* **2**(11): 1500101 (2015)

[22] Berman D, Erdemir A, Sumant A V. Graphene: A new emerging lubricant. *Mater Today* **17**(1): 31–42 (2014)

[23] Sun C B, Feng Y Y, Li Y, Qin C Q, Zhang Q Q, Feng W. Solvothermally exfoliated fluorographene for high-performance lithium primary batteries. *Nanoscale* **6**(5): 2634–2641 (2014)

[24] Mazánek V, Jankovský O, Luxa J, Sedmidubský D, Janoušek Z, Šembera F, Mikulics M, Sofer Z. Tuning of fluorine content in graphene: Towards large-scale production of stoichiometric fluorographene. *Nanoscale* **7**(32): 13646–13655 (2015)

[25] Boopathi S, Narayanan T N, Kumar S S. Improved heterogeneous electron transfer kinetics of fluorinated graphene derivatives. *Nanoscale* **6**(7): 10140–10146 (2014)

[26] Lu A H, Hao G P, Sun Q. Can carbon spheres be created through the stöber method? *Angew Chem Int Ed* **50**(39): 9023–9025 (2011)

[27] Fan X Q, Wang L P. Highly conductive ionic liquids toward high-performance space-lubricating greases. *ACS Appl Mater Interfaces* **6**(16): 14660–14671 (2014)

[28] O'Hagan D. Understanding organofluorine chemistry. An introduction to the C–F bond. *Chem Soc Rev* **37**(2): 308–319 (2008)

[29] Sato Y, Kume T, Hagiwara R, Ito Y. Reversible intercalation of HF in fluorine–GICs. *Carbon* **41**(2): 351–357 (2003)

[30] Urbanová V, Karlický F, Matěj A, Šembera F, Janoušek Z, Perman J A, Ranc V, Čépe K, Michl J, Otyepka M, et al. Fluorinated graphenes as advanced biosensors-effect of fluorine coverage on electron transfer properties and adsorption of biomolecules. *Nanoscale* **8**(24): 12134–12142 (2016)

[31] Lyth S M, Ma W, Liu J, Daio T, Sasaki K, Takahara A,

Ameduri B. Solvothermal synthesis of superhydrophobic hollow carbon nanoparticles from a fluorinated alcohol. *Nanoscale* **7**(38): 16087–16093 (2015)

[32] Nebogatikova N A, Antonova I V, Prinz V Y, Kurkina I I, Vdovin V I, Aleksandrov G N, Timofeev V B, Smagulova S A, Zakirov E R, Kesler V G. Fluorinated graphene dielectric films obtained from functionalized graphene suspension: Preparation and properties. *Phys Chem Chem Phys* **17**(20): 13257–13266 (2015)

[33] Yang K, Wan J M, Zhang S, Zhang Y J, Lee S T, Liu Z. In vivo pharmacokinetics, long-term biodistribution, and toxicology of PEGylated graphene in mice. *ACS Nano* **5**(1): 516–522 (2011)

[34] Alazemi A A, Dysart A D, Phuah X L, Pol V G, Sadeghi F. MoS_2 nanolayer coated carbon spheres as an oil additive for enhanced tribological performance. *Carbon* **110**: 367–377 (2016)

[35] Zhang L L, Pu J B, Wang L P, Xue Q J. Synergistic effect of hybrid carbon nanotube−graphene oxide as nanoadditive enhancing the frictional properties of ionic liquids in high vacuum. *ACS Appl Mater Interfaces* **7**(16): 8592–8600 (2015)

[36] Fan X Q, Li W, Fu H M, Zhu M H, Wang L P, Cai Z B, Liu J H, Li H. Probing the function of solid nanoparticle structure under boundary lubrication. *ACS Sustainable Chem Eng* **5**(5): 4223–4233 (2017)

[37] Fan X Q, Wang L P. High-performance lubricant additives based on modified graphene oxide by ionic liquids. *J Colloid Interface Sci* **452**: 98–108 (2015)

[38] Tillmanns E, Gebert W, Bau W H. Computer simulation of crystal structures applied to the solution of the superstructure of cubic silicondiphosphate. *J Solid State Chem* **7**(1): 69–84 (1973)

[39] Liu X F, Pu J B, Wang L P, Xue Q J. Novel DLC/ionic liquid/graphene nanocomposite coatings towards high-vacuum related space applications. *J Mater Chem A* **1**(11): 3797–3809 (2013)

[40] Mu Z G, Zhou F, Zhang S X, Liang Y M, Liu W. Effect of the functional groups in ionic liquid molecules on the friction and wear behavior of aluminum alloy in lubricated aluminum-on-steel contact. *Tribol Int* **38**(8): 725–731 (2005)

[41] Nair R R, Ren W, Jalil R, Riaz I, Kravets V G, Britnell L, Blake P, Schedin F, Mayorov A S, Yuan Y, et al. Fluorographene: A two-dimensional counterpart of teflon, *Small* **24**(6): 2877–2884 (2010)

Xiaojing CI. She received her bachelor degree in material science and engineering in 2017 from Nanjing Technology University, Nanjing, China. After then, she is a master student in Shanghai University. Her research interests include 2D-materials and lubrication.

Wenjie ZHAO. He received his Ph.D. degree in materials science from Lanzhou Institute of Chemical Physics (LICP), Chinese Academy of Sciences (CAS), China, in 2010. Then, he joined the Key Laboratory of Marine Materials and Related Technologies at Ningbo Institute of Materials Technology and Engineering, CAS, China. His current position is a professor. His research areas cover the tribology of composite materials, 2D nanomaterials preparation, interfacial physical chemistry, and protective coatings.

Jun LUO. He received his Ph.D. in condensed matter physics from the Institute of Physics, CAS, China, in 2005. Then, he was awarded an Alexander von Humboldt Research Fellowship to visit Free University of Berlin, Germany. He went back to Institute of Physics, CAS, in 2007, and worked there for about 7 years. In October of 2013, he transferred to Shanghai University and continued his work on thermoelectric materials.

Yangmin WU. He received his bachelor and master degrees from Jiangxi University of Science and technology, China, in 2015 and 2019, respectively. Now, he is a Ph.D. student in the Key Laboratory of Marine Materials and Related Technologies at Ningbo Institute of Materials Technology and Engineering, CAS. His research interests mainly focus on synthesis and application of 2D nanomaterials.

Tianhao GE. She received her bachelor degree in material shaping and control engineering in China University of Petroleum (East China), Qingdao, China. After then, she is a master student in the joint training Master of Science Program provided by Shanghai University and Ningbo Institute of Materials Technology and Engineering, CAS. Her research interest mainly focuses on the marine functional materials.

Qunji XUE. He graduated from the Chemistry Department, Shandong University in 1965, and received his master degree from LICP, CAS, China, in 1967. He has been working in LICP since 1967. He was elected as the member of the Chinese Academy of Engineering in 1997. From 2012, he joined the Ningbo Institute of Materials Technology and Engineering, CAS. He was awarded title of HeLiangHeLi Foundation Science and Technology Progress Prize (2002), Supreme Achievement Award in Tribology (2009), and Tribology Gold Medal (2011). He has presided over or participated in about 30 national major research programs, and published more than 300 papers and 3 monographs.

Zhiwen FANG. He received his bachelor degree in Tianjin University, China, in 1985, and got his M.Eng. degree from Tianjin University. Now, he is vice chairman, general manager, and technical director of Shandong Chongshan photoelectric materials Co., Ltd., part-time professor of Tianjin University and Shandong University of technology, member of fluorine-containing gas sub Technical Committee of National Gas Standardization Technical Committee, director of lithium battery branch of China chemical and physical power industry association, and has been engaged in the development and research of semiconductor and new energy materials.

Xiulei GAO. He received his bachelor degree in applied chemistry from Qilu University of Technology, China, in 2010. Now, he is the director of Department General Fluorocarbon Materials Project of Shandong Chongshan photoelectric materials Co., Ltd. His research focuses on surface treatment, smart coating, and tribology.